Weather and Climate Extremes 19 (2018) 1–9

Contents lists available at ScienceDirect

Weather and Climate Extremes

journal homepage: www.elsevier.com/locate/wace

Drivers of 2016 record Arctic warmth assessed using climate simulations subjected to Factual and Counterfactual forcing

Lantao Sun [a,*], Dave Allured [a], Martin Hoerling [b], Lesley Smith [a], Judith Perlwitz [a], Don Murray [a], Jon Eischeid [a]

[a] Cooperative Institute for Research in Environmental Sciences, University of Colorado at Boulder and NOAA Earth System Research Laboratory, Boulder CO 80305, USA
[b] NOAA Earth System Research Laboratory, Boulder CO 80305, USA

ARTICLE INFO

Keywords:
Arctic
Climate
Extreme
Model
Attribution

ABSTRACT

A suite of historical atmospheric model simulations is described that uses a hierarchy of global boundary forcings designed to inform research on the detection and attribution of weather and climate-related extremes. In addition to experiments forced by actual variations in sea surface temperature, sea ice concentration, and atmospheric chemical composition (so-called Factual experiments); additional (Counterfactual) experiments are conducted in which the boundary forcings are adjusted by removing estimates of long-term climate change. A third suite of experiments are identical to the Factual runs except that sea ice concentrations are set to climatological conditions (Clim-Polar experiments). These were used to investigate the cause for extremely warm Arctic surface temperature during 2016.

Much of the magnitude of surface temperature anomalies averaged poleward of 65°N in 2016 (3.2 ± 0.6 °C above a 1980–89 reference) is shown to have been forced by observed global boundary conditions. The Factual experiments reveal that at least three quarters of the magnitude of 2016 annual mean Arctic warmth was forced, with considerable sensitivity to assumptions of sea ice thickness change. Results also indicate that 30–40% of the overall forced Arctic warming signal in 2016 originated from drivers outside of the Arctic. Despite such remote effects, the experiments reveal that the extreme magnitude of the 2016 Arctic warmth could not have occurred without consideration of the Arctic sea ice loss. We find a near-zero probability for Arctic surface temperature to be as warm as occurred in 2016 under late-19th century boundary conditions, and also under 2016 boundary conditions that do not include the depleted Arctic sea ice. Results from the atmospheric model experiments are reconciled with coupled climate model simulations which lead to a conclusion that about 60% of the 2016 Arctic warmth was likely attributable to human-induced climate change.

1. Introduction

NOAA's Arctic Report (Overland et al., 2016a) indicated that the annual surface air temperature anomaly in 2016 for land areas north of 60°N far exceeded the highest in the observational record since 1900. Further, the 2016 anomaly was double the magnitude during just the prior year. In this study, a set of historical climate model simulations are introduced that contribute to the Climate of the Twentieth Century Detection and Attribution Project (Folland et al., 2014). These simulations are used to determine the drivers of extreme Arctic warmth in 2016.

Record setting Arctic warmth in 2016 did not come entirely as a surprise. A prolonged warming of annual Arctic surface temperatures has been observed since the late 1970s (Overland et al., 2016a), despite appreciable superposed intrinsic decadal variability (e.g. Polyakov et al., 2002). The recent Arctic warming has occurred in tandem with temperature rises in middle and lower latitudes, suggesting that it is part of an overall global warming pattern (e.g. Serreze and Francis, 2006). Most of the Arctic warming since 1979 has occurred during fall and winter, with observational studies (e.g. Screen and Simmonds, 2010) and climate model experiments (e.g. Screen et al., 2013a, b; Perlwitz et al., 2015) indicating sea ice loss to have been a major driver. Given that 2016 Arctic sea ice extent was itself near a record low,[1] boundary conditions were conducive for high Arctic surface temperatures.

* Corresponding author. 325 Broadway, R/PSD1 Boulder, CO 80305-3328, USA
E-mail address: lantao.sun@noaa.gov (L. Sun).

[1] Record low monthly extents were set in January, February, April, May, June, October, and November. http://nsidc.org/arcticseaicenews/2017/01/low-sea-ice-extent-continues-in-both-poles/.

https://doi.org/10.1016/j.wace.2017.11.001
Received 13 July 2017; Received in revised form 7 November 2017; Accepted 12 November 2017
Available online 6 December 2017
2212-0947/© 2017 The Authors. Published by Elsevier B.V. This is an open access article under the CC BY-NC-ND license (http://creativecommons.org/licenses/by-nc-nd/4.0/).

Lest the impression be that extreme Arctic warmth was unavoidable and that the record-setting conditions in 2016 could have been readily anticipated, several lines of evidence also indicate an appreciable random, unforced contribution. For instance, multi-model simulations of the Coupled Model Intercomparison Project (CMIP5) were used to examine how global warming contributed to the remarkable November–December 2016 warmth near the North Pole (van Oldenborgh et al., 2017). Results indicated that the magnitude of warmth was an extreme condition relative to the global warming signal itself, and as such was a low probability outcome in 2016. Likewise, Kim et al. (2017) examined impacts of intense Storm Frank during January 2016 when daily Arctic surface temperatures were as much as 30 °C above average, revealing the importance of weather-driven heat and moisture transports.

Quantifying the effects of various drivers is central to explaining how extreme Arctic warmth can arise, to understanding why it happened in 2016 specifically, and to better anticipating future occurrences of extreme Arctic events. In this study we first pose the question whether the magnitude of the observed annual surface air temperature anomalies averaged poleward of 65°N were reconcilable with boundary forcing during 2016 alone using a unique set of atmospheric model simulations. Our modeling approach should be distinguished from a purely CMIP5 approach (e.g. van Oldenborgh et al., 2017) in so far as the particular observed ocean and sea ice conditions of 2016 are treated as forcings in the model experiments used herein. We then inquire about the character of the boundary forcing by using a set of experiments driven by realistic and idealized representations of global boundary conditions. Among various questions these experiments address, one focuses upon whether the extreme warmth arose mostly from drivers within or outside of the Arctic. We also explore the extent to which the extreme articulation of 2016 Arctic warmth may have resulted from an appreciable impetus provided by purely random variability. It is apparent from synoptic analysis of Arctic weather conditions in 2016 (e.g. Kim et al., 2017; Overland and Wang, 2016) that weather driving was important, and that such weather driving likely affected the sea ice boundary conditions. Thus, consistent with estimates that about 40% of Arctic sea ice loss since 1979 is due to internal atmospheric variability (Ding et al., 2017), estimates of the random component of 2016 warmth must address such internal coupled feedbacks. Our analysis therefore also examines coupled model simulations that span the same historical record as our atmospheric simulations, and which involve large ensembles to facilitate diagnosis of the magnitude for internal coupled noise.

We describe in Section 2 our suite of atmospheric model simulations that employ boundary forcings representative of 2016 conditions for a factual (observed) and counterfactual (absent long-term climate change) world. The rationale is to create an experimental dataset, routinely updated and made available to the broader scientific community, that can be used to isolate contributions of specific drivers to observed climate variability and extreme events. The experimental methods involve large ensemble simulations for each configuration of boundary forcing, thereby permitting diagnosis of contributions by various drivers and also by internal atmospheric variability. A feature of the experimental suite is that in addition to runs forced by the actual variations in sea surface temperature, sea ice concentration, and atmospheric chemical composition (the standard Atmospheric Model Intercomparison Project (AMIP) configuration); additional experiments are conducted in which the boundary forcings are adjusted by removing plausible estimates of the effects of long-term climate change. Section 2 describes how these counterfactual boundary conditions were constructed and addresses implications of various simplifying assumptions.

The application of these experiments toward an attribution of the 2016 extreme Arctic warmth is presented in Section 3. It is demonstrated that roughly three quarters of the magnitude of 2016 annual mean Arctic warmth was likely a forced signal owing to the particular global ocean boundary conditions. Of this forced signal, about 30–40% likely arose from drivers outside of the Arctic, while Arctic sea ice loss accounted for 60–70% with estimates sensitive to assumptions of sea ice thickness change. The Discussion section compares results on the drivers of 2016 Arctic warmth drawn from our atmospheric model experiments with results using transient coupled climate model simulations.

2. Observed data and model experiments

2.1. Observations

Near-surface air temperatures are based on five reanalysis products — NCEP/NCAR (R1; Kalnay et al., 1996), ERA-Interim (Dee et al., 2011), NASA-MERRA-2 (Gelaro et al., 2017), and two versions of JRA-55 analyses that involve different treatments of the near-surface air temperature (Kobayashi et al., 2015). The common period for these products is 1980–2016. Annual surface air temperatures are area-averaged for the region 65°N-90°N, and anomalies are calculated with respect to each product's 1980-89 mean.

Two sea surface temperature (SST) data sets are used to investigate long-term change since 1880. We use the NOAA Extended Reconstructed Sea Surface Temperature v3 (ERSSTv3) (Smith et al., 2008), results from which are compared to the Hadley Center Global Sea Ice and Sea Surface Temperature v1 (HadISSTv1) data (Rayner et al., 2003).

2.2. Atmospheric model and experiments

The atmospheric model used in support of the Climate of the 20th Century Detection and Attribution Product is the European Center for Medium Range Weather Forecast/Hamburg (ECHAM5) model (Roeckner et al., 2003). The model is run at a spectral resolution of T159 (~85 km horizontal resolution) and 31 vertical levels having a model top at about 1 hPa.

In its standard AMIP configuration (hereafter, Factual experiment), ECHAM5 is forced by specifying observed monthly variations in SST and sea ice concentration as derived from Hurrell et al. (2008). Greenhouse gases (GHGs) vary according to the observed concentrations and their extension after 2005 assuming Representative Concentration Pathway 6.0 (RCP6.0) (Meinshausen et al., 2011). Monthly evolving tropospheric and stratospheric ozone also vary based on Cionni et al. (2011). Aerosol concentrations do not vary interannually in ECHAM5, and a specified repeating seasonal cycle is derived from an aerosol model described in Tanre et al. (1984). The experiments are from January 1979–December 2016. A 30-member ensemble of simulations is generated in which each member experiences identical time evolving boundary forcings, but is begun from different atmospheric initial states in January 1979.

Two additional parallel experiments are performed in which the boundary and external forcings are modified. In one suite (hereafter, Counterfactual experiment), the model is forced with monthly varying boundary conditions that retain the interannual and decadal variability as occurring in the Factual experiment, but in which the long-term trends in the boundary forcings have been removed. For external radiative forcing in these Counterfactual experiments, GHG and ozone concentrations are simply set to their 1880 values. For the SSTs, an approximation of 1880 conditions is generated by removing a 1880–2011 linear SST trend from the monthly variability. Sea ice concentrations are set to a 1979–1989 climatological mean globally, a period that mostly precedes the time of substantial decline in Arctic sea ice that culminated in the near-record low concentrations during 2016. In the second suite (hereafter, Clim-Polar experiment), all boundary conditions and external radiative forcings are identical to those specified in the Factual runs, except that global sea ice concentrations are set to a 1979–1989 climatological mean. Each suite spans 1979–2016 and includes 30-member ensembles. Table 1 summarizes these three sets of experiments and their specified boundary forcings.

When diagnosing the 2016 Arctic extreme warmth, the model spread is represented by the 95% confidence bound across 30 members of simulations based on student's t-test. The contribution from the drivers

Table 1
The various ECHAM5 simulations used in this study, and description of the radiative forcing and lower boundary conditions for each experiment.

Experiments	Radiative Forcing (including O_3)	Sea Surface Temperature (SST)	Sea Ice Concentration
Factual	1979–2016[a]	1979–2016	1979–2016
Counterfactual	1880	Residual 1979–2016[b]	Climatology 1979–1989 Mean
Clim-Polar	1979–2016[a]	1979–2016 except over the Arctic[c]	Climatology 1979–1989 Mean

[a] From 1979 to 2005, the observed radiative forcing is used; from 2006 to 2016 the RCP6.0 radiative forcing is used.
[b] In Counterfactual experiment, an approximation of pre-industrial SST condition is generated by removing a 1880–2011 linear zonal-mean SST trend from the 1979–2016 monthly data. The purpose is to remove the observed SST warming trend while retaining the SST variability. See section 2.2, 2.3 for details.
[c] In Clim-Polar experiment, the observed SSTs are prescribed from 1979 to 2016 except in the Arctic sea ice loss region, where the 1979–1989 climatology is used as consideration for the sea ice loss-induced SST increase. See Perlwitz et al. (2015) for details.

outside of the Arctic to the total 2016 extreme warmth is estimated by the ratio of the ensemble mean of the Clim-Polar to the Factual experiment.

2.3. Counterfactual boundary conditions

Various assumptions in constructing the counterfactual forcings were made. One is that the long-term SST change can be described by a linear trend since 1880. Fig. 1 (top) shows the time series of the globally averaged annual SSTs for 1880–2016, and the red curve denotes the 1880–2011 linear trend. (We note that this linear fit was computed from available data up to commencement of our experiments in 2012, and for consistency with our regular updates through time, we extend this trend to recent years rather than re-calculate and update the trend annually.) Our linear fit to the time series underestimates the magnitude of SST warmth post-1990. As such our estimates of the long-term climate change contribution to the recent 2016 extreme conditions may likewise be underestimated.

We use the ERSSTv3b data to estimate the long-term trend, and there are appreciable differences among SST data sets. Fig. 2 compares the 1880–2011 linear trend in annual SSTs using the NOAA ERSSTv3b data (top) with the HadISSTv1 data (middle). Left-side panels show trends computed at each grid point, and the right-side panels show the zonal averages of the SST trends. For the former metric, differences in trends are substantial, including equatorial central Pacific cooling in HadISSTv1 compared to warming in the ERSSTv3b. We utilize the latter data set in part because of indications of long-term warming in the equatorial eastern Pacific based on examination of uninterpolated SST and marine air temperature data sets (Deser et al., 2010), but the uncertainty in regional SST trend patterns over the eastern equatorial Pacific is high (e.g. Solomon and Newman, 2012).

Given this uncertainty in the pattern of SST change since 1880, and the confounding issue that local trend features can be prone to effects of internal variability, our approach in constructing the counterfactual is to remove the 1880–2011 trend in *zonal mean SSTs* from the actual observed SSTs. The zonal mean patterns of the ERSSTv3b are quite similar to those occurring in the average of the 37-member so-called "All-

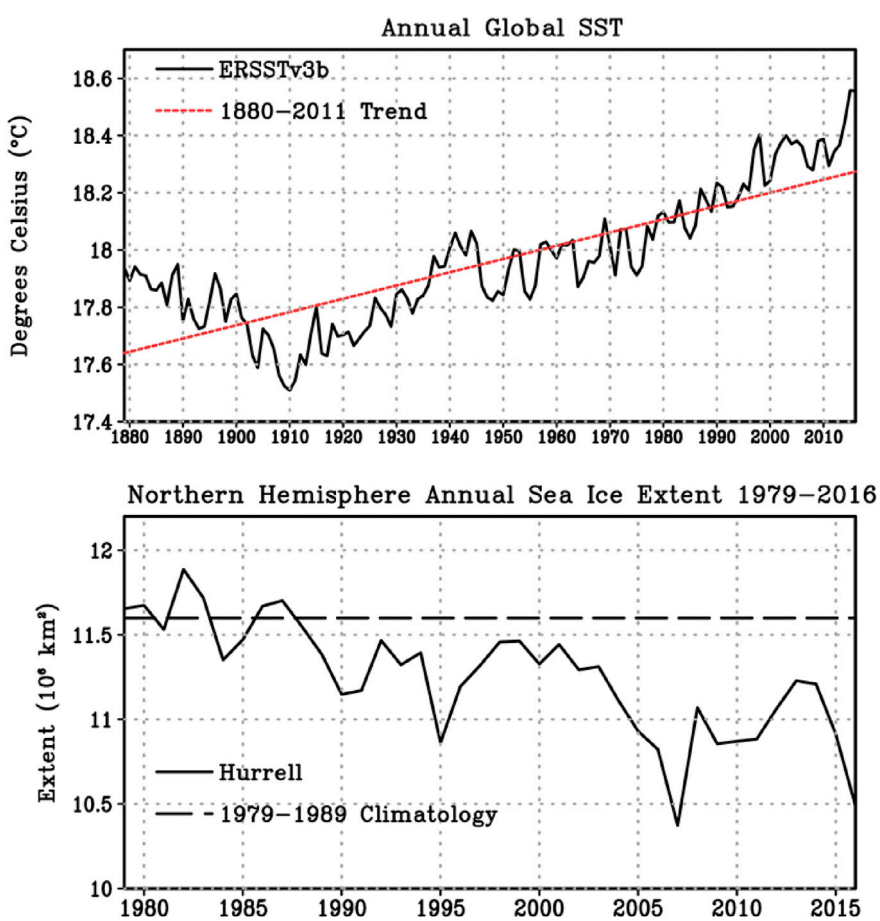

Fig. 1. (Top) Time series of observed globally averaged annual SST (black curve; °C) and its 1880–2011 linear trend (red curve). (Bottom) Time series of annual Arctic sea ice extent (solid curve; 10^6 km^2) and its 1979–1989 climatology (dashed curve).

Forcings" experiments of CMIP5 (Fig. 2, bottom) suggesting that the former is consistent with a pattern of externally forced change. Nonetheless, it should be stressed that herein we use a single SST change pattern in creating the counterfactual forcing that is specified in our ECHAM5 experiments. Other assumptions on long-term change in boundary conditions could be made; however, it is beyond the scope of the current study to address this source of uncertainty (see also Christidis et al., 2013).

Regarding the counterfactual assumption of Arctic sea ice extent change, it is evident from the annual sea ice time series (Fig. 1, bottom) that most of the decline occurs post-1990. We therefore use a reference sea ice condition of 1979-89 to denote the period of Arctic boundary forcing that is mostly antecedent to appreciable climate change. This choice is a compromise to take advantage of a consistent satellite-era record of high quality sea ice observations since 1979 which likely captures the majority of long-term decline (Walsh et al., 2016) versus attempting to estimate late-19th century sea ice from sparse and much less reliable data. A further aspect of sea ice change involves ice thickness. In each of the three suites of ECHAM5 experiments, sea ice thickness is assumed to be a constant 2 m value that is invariant through time during 1979–2016. Yet, analysis of data from the Pan-Arctic Ice Ocean Modeling and Assimilation System (PIOMAS, Zhang and Rothrock, 2003) indicates that sea ice thickness was substantially reduced in 2016 compared to a 1980–89 reference (Fig. S1 in the supplementary material), and previous modeling studies point to a sensitivity of atmospheric response to prescribed thickness changes especially during winter (Rinke et al., 2006; Krinner et al., 2010; Lang et al., 2017). To address the sensitivity of our Factual experiment results to sea ice thickness decline, an additional 30-member Factual experiment is conducted, covering 2016, in which sea ice thickness is reduced to 1 m at all locations having sea ice concentration. While this is an idealization of the PIOMAS spatial maps and their temporal evolution, the comparison of the 2 m to the 1 m sea ice thickness results nonetheless gives a measure of uncertainty in our estimate of the forced component of 2016 Arctic warmth.

3. Drivers of 2016 extreme Arctic warmth

Fig. 3a presents time series of Arctic (65°N - 90°N) annual surface air temperature anomalies relative to a 1980–1989 climatology from the five reanalysis datasets and from the 30-member ensemble of ECHAM5 Factual experiments. The reanalyses and simulations show an overall Arctic warming since 1980 with a high temporal correlation (0.89) indicative of a strongly forced warming trend. In 2016, the average of the reanalysis products (red curve) indicates an Arctic surface air temperature anomaly of 3.2 ± 0.6 °C (95% confidence interval) while the ensemble mean simulated anomaly is 2.4 ± 0.1 °C in the Factual experiment with 2 m ice thickness. There is considerable analysis uncertainty, with the range among the five reanalysis products being 2.4 °C–3.7 °C. This range is large compared to the 0.25 °C standard deviation among individual members of the model simulations.

A stronger warming is simulated in ECHAM5 when also considering effects of sea ice thinning. Repeating the Factual experiment but specifying 1 m rather than 2 m sea ice thickness yields a 2016 Arctic surface air temperature anomaly of 3.1 ± 0.1 °C (blue star). This additional warming effect in 2016 is in qualitative agreement with Lang et al. (2017), who also found sea ice thinning to cause enhanced near-surface warming in their atmospheric model simulations. We emphasize, however, that our treatment of sea ice thickness is highly simplified in both Factual experiments in so far as neither includes a seasonal cycle or a spatial pattern

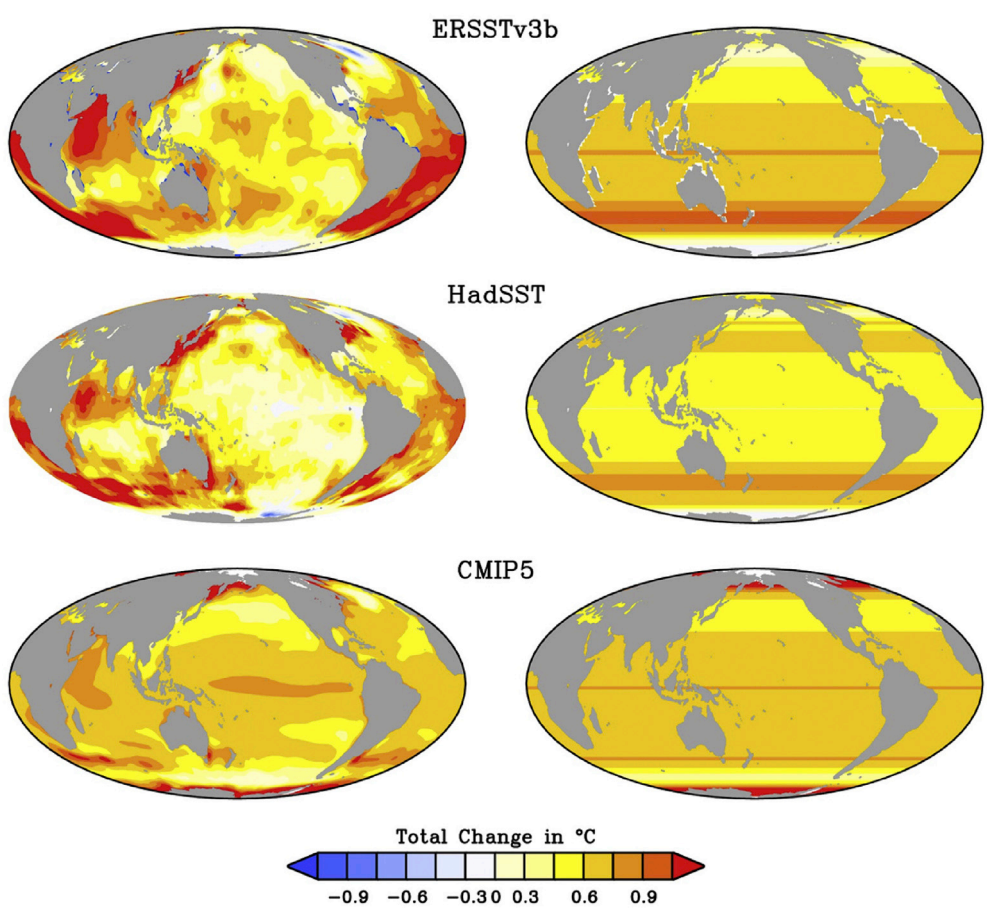

Fig. 2. 1880–2011 linear SST trend (°C) computed at each grid point (left) and zonal-average (right) from ERSSTv3b (top), HadiSSTv1 (middle) and ensemble mean of the 37 CMIP5 models subjected to "All Forcings" during historical period and RCP8.5 emission scenario after 2005 (bottom).

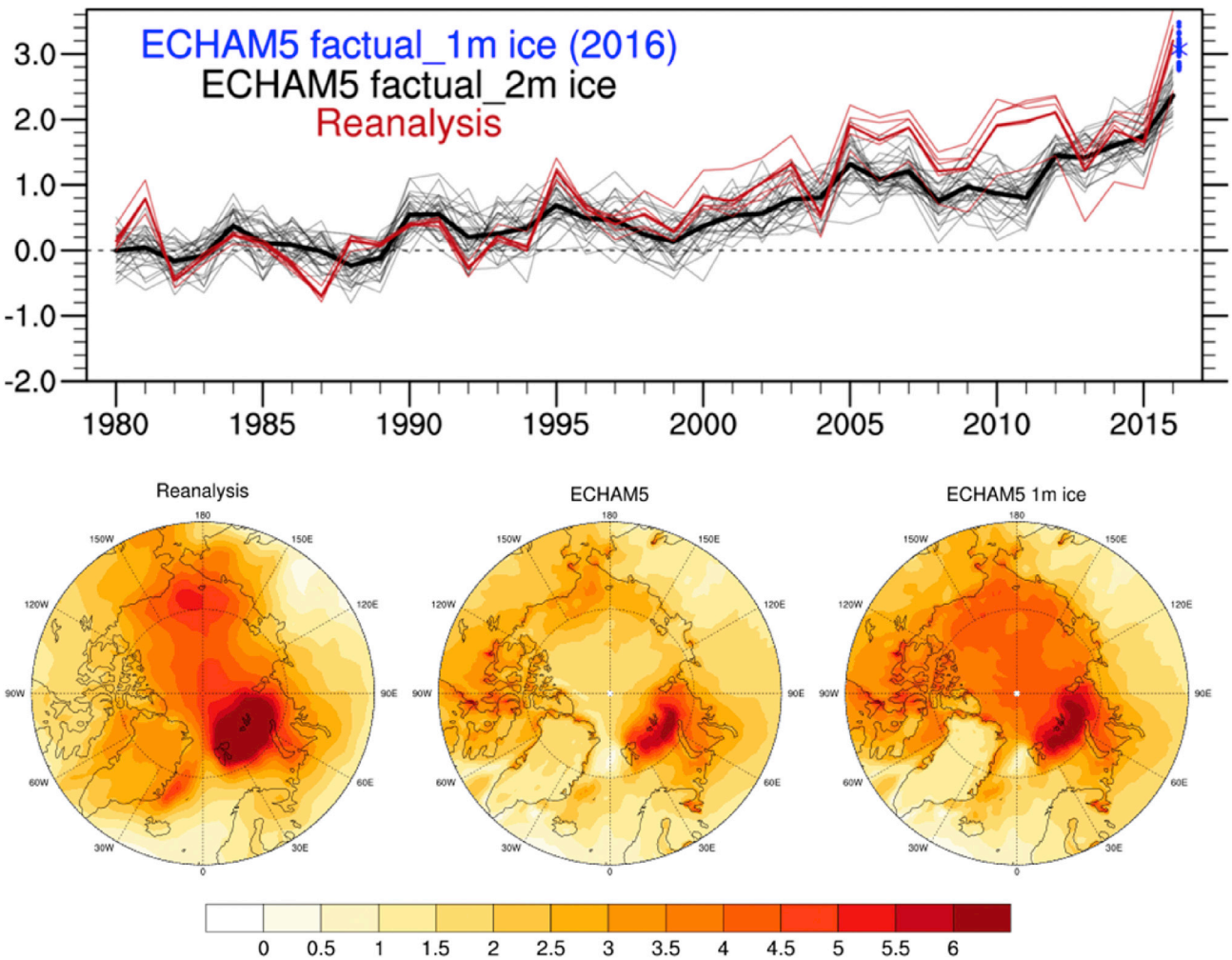

Fig. 3. (Top) Time series of Arctic surface temperature anomaly (°C) relative to the 1980–1989 climatology for the ECHAM5 Factual experiments (thin black curves: individual ensembles; thick black curve: ensemble mean) and reanalysis datasets (thin red curves: five reanalysis results; thick red curve: average). Blue asterisk denotes the 2016 ensemble mean anomaly from the Factual experiments with 1 m ice thickness and blue dots show the individual ensemble values. (Bottom) 2016 Arctic surface temperature anomalies from the reanalysis average (left), Factual experiments with 2 m ice thickness (middle) and with 1 m ice thickness (right).

to sea ice thickness variability.

Despite those limitations, various features of the spatial structure in the 2016 warmth across the Arctic is well captured in the experiments (Fig. 3, lower panels). For instance, both reanalysis (left) and the Factual experiment (middle) have the largest warm anomaly over the Barents-Kara Sea region. Warm anomalies over the Arctic Ocean tend to exceed those over Arctic land regions in the average of reanalysis products, which is different from the more uniform warmth in the Factual experiment with 2 m ice thickness. Results from the Factual runs with 1 m ice thickness, however, yields appreciably greater warming over the Arctic Ocean (right) that is in closer spatial agreement with the reanalysis product. When averaged over the Arctic as a whole, our Factual experiments indicate about 75% ± 3% of the observed 2016 warmth was forced, with an even larger fraction resulting from boundary forcing when accounting for sea ice thinning effects.

A substantial contribution to 2016 Arctic warmth originated from drivers outside of the Arctic. Fig. 4 compares the 1979–2016 Arctic surface air temperature time series in the Factual experiment (repeated for clarity in Fig. 4, top) with those in the Clim-Polar experiment (Fig. 4, middle). A 1.0 ± 0.1 °C warm anomaly in 2016 occurs in the Clim-Polar ensemble average, accounting for roughly 30–40% of the warm anomaly in the Factual experiments (depending on sea ice thickness change assumptions). While it is beyond the scope of this paper to determine the physical mechanisms for the warm signal resulting from these lower latitudes drivers, we speculate that most of the Arctic warming in the Clim-Polar experiments is due to SST warming of the world oceans. The effect of that would plausibly lead to a poleward atmospheric transport of the resultant increased atmospheric sensible and latent energy. Likewise, an overall rise in atmospheric water vapor associated with ocean warming outside the Arctic could lead to increased Arctic water vapor via transports from lower latitudes, again inducing Arctic warming but via a mechanism of anomalous downwelling longwave radiation (e.g. Franzke et al., 2017). It is also possible that lower latitude atmospheric circulations themselves changed in response to warming oceans, either because of internal multi-decadal variability or external forcing, again acting to increase the poleward heat transport into the Arctic (e.g. Perlwitz et al., 2015).

Regardless of the mechanism, the key point of Fig. 4 is that the spread among 30-member Clim-Polar runs is small. As such the extreme 2016 Arctic warmth cannot be reconciled with drivers originating from outside of the Arctic alone. No single member of the Clim-Polar experiment yields a 2016 Arctic warm anomaly as large as any of the reanalysis product estimates. The results thus indicate changes in Arctic boundary conditions were necessary for explaining the extreme event. Of course, those boundary conditions during 2016, especially near-record sea ice depletion, may themselves have been appreciably perturbed by drivers from outside the Arctic in 2016 (see Introduction). An atmospheric modeling approach alone, however, is unable to disaggregate such

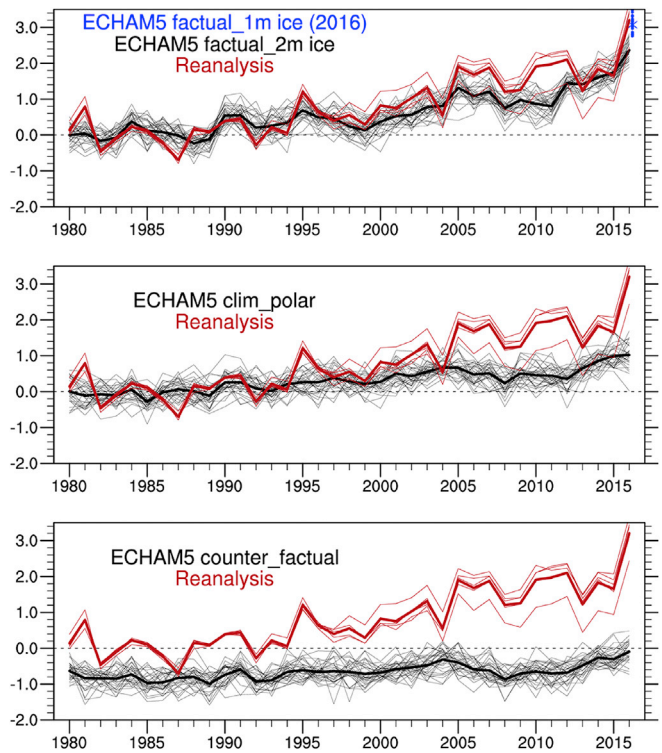

Fig. 4. Time series of Arctic surface temperature anomaly (°C; black curves) for the ECHAM5 Factual (top), Clim-Polar (middle) and Counterfactual experiments (bottom). The anomalies are calculated relative to the 1980–1989 climatology of the Factual experiments. The thin black curves denote the individual ensembles while the thick black curve indicates the 30- member ensemble-mean. The reanalysis results are superimposed in all three panels for comparison (thin red curves: five reanalysis products; thick red curve: reanalysis average). In top panel, blue asterisk denotes the 2016 ensemble mean anomaly from the Factual experiments with 1 m ice thickness and blue dots show the individual ensemble values.

coupled interactions, and we will return to the question of coupled variability in the paper's last section.

In the absence of long-term climate change (i.e. no changes in SSTs, sea ice, and external radiative forcing), Arctic surface air temperatures in 2016 would not have been appreciably different from their late 19th century climatological values. The time series of Arctic surface air temperature anomalies simulated in the Counterfactual experiments (Fig. 4, bottom) are consistently colder than the 1980-89 climatological mean of the Factual experiment. The roughly 0.75 °C cold anomaly during the first few years of the simulation reveals the magnitude of the Arctic climate change signal (1880–1980) in our experiment. There is some modest decadal variability in Arctic surface air temperatures during 1980–2016 overall in the Counterfactual runs, though these are weak in amplitude indicating that natural variability of boundary forcings such as might arise from natural El Niño-Southern Oscillation (ENSO) cycles or Pacific decadal SST variations could not have appreciably contributed to 2016 extreme Arctic warmth. We note also that there is a slight warming trend of Arctic surface temperatures in the Counterfactual experiments. This feature is likely a climate change signal rather than a symptom of internal natural variability owing to our assumptions for defining the counterfactual SSTs (see Section 2).

Moreover, to depict the uncertainty arising from the use of different models, we have repeated our analysis using a second model – Community Atmosphere Model Version 5 (CAM5; Neale et al., 2010). The CAM5 experiments follow the protocol of the ECHAM5 experiments using the same forcing and surface boundary conditions. Figure S2 shows the time series of Arctic annual surface air temperature anomalies from the ensemble of CAM5 Factual, Clim-Polar and Counterfactual experiments. The forced signal of 2016 Arctic surface temperature anomaly is 2.8 ± 0.1 °C in the CAM5 Factual experiments and is 1.4 ± 0.1 °C in the CAM5 Clim-Polar experiments, implying that drivers outside the Arctic explain half of the total temperature change. These findings are qualitatively in agreement with the ECHAM5 results, establishing the robustness of our AMIP experiments.

To further characterize the 2016 extreme Arctic warmth, we plot in Fig. 5 the frequency distributions of annual surface temperature comprised of the ECHAM5 individual 30 runs for each of the four simulations that employ various boundary forcings. The result reveals a progressive increase in the magnitude of Arctic warmth as more features of the actual 2016 boundary forcings are incorporated into the experiments. Neither the Counterfactual nor the Clim-Polar experiments yield a statistical probability of 2016 Arctic surface temperatures that is consistent with the observations, even when accounting for the considerable uncertainty in the actual magnitude of the 2016 Arctic warmth (see tick marks in Fig. 5). In other words, the probability for Arctic surface temperature as large as occurred in 2016 is effectively nil under late-19th century boundary conditions and also under 2016 boundary conditions that fail to include the 2016 state of depleted Arctic sea ice volume. Under the more realistic assumption of a reduction in Arctic sea ice extent (but no change in sea ice thickness), the observed 2016 Arctic warmth falls within the population sample of Factual (2 m ice) simulations, though having a low probability outcome. Those experiments would require one to invoke the presence of a strong articulation of internal atmospheric variability during 2016, in addition to a strong boundary forced warmth, to explain the observed extreme event. Yet, when incorporating a reduction in sea ice thickness, the extreme magnitude of the 2016 warmth is found to be close to the mean value of the probability distribution of the Factual (1 m ice) simulations. Those experiments indicate the observed extreme event was almost entirely a forced response to boundary conditions, though we caution that some

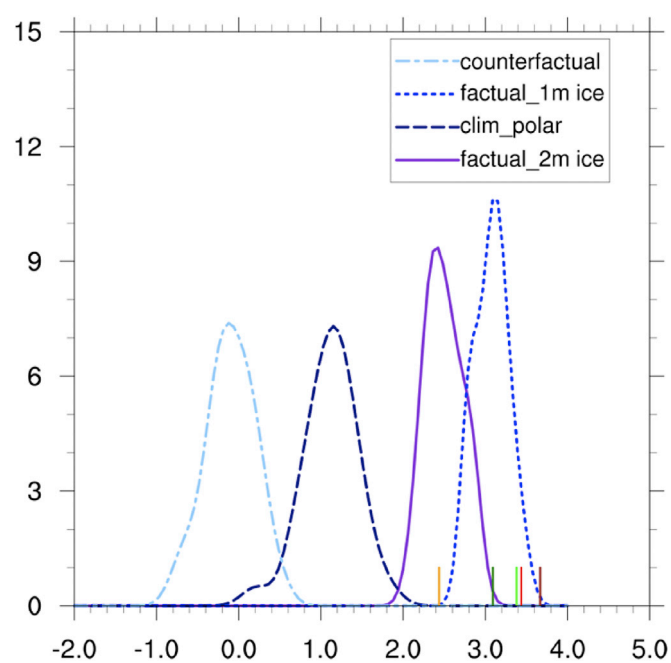

Fig. 5. Probability density functions (PDFs) for the 2016 Arctic surface temperature anomaly (°C) in various ECHAM5 simulations. The anomalies are calculated relative to the 1980–1989 climatology of the Factual experiments. The five reanalysis results are denoted by tick marks (light brown for MERRA-2; forest green for JRA-55; light green for JRA-55(Screen); red for ERA-Interim; dark brow for NCEP/NCAR reanalysis). The PDFs are the non-parametric estimates of the frequency distributions based on Kernal density, and have been smoothed using a Gaussian filter.

Table 2
2016 Arctic near-surface air temperature anomalies (°C) in the reanalysis and ECHAM5 ensemble means averaged annually (ANN) and over four seasons [January-February-March (JFM); April-May-June (AMJ); July-August-September (JAS); October-November-December (OND)].

	ANN	JFM	AMJ	JAS	OND
Reanalysis average	3.2	4.2	2.6	1.8	4.2
Factual (1-m ice)	3.1	4.4	1.7	1.3	4.8
Factual (2-m ice)	2.4	2.7	1.4	1.2	4.0
Clim-Polar	1.1	1.4	1.0	0.7	1.2
Counterfactual	−0.1	−0.1	−0.1	−0.2	0.0

fraction of the sea ice conditions in particular may nonetheless represent effects of internal climate drivers rather than being symptoms solely of long-term climate change.

In addition to the annual mean temperature diagnostics, we also examined the seasonal contributions to the 2016 extreme warmth in ECHAM5 by calculating the Arctic surface temperature anomalies and the model-based estimates of different physical contributions for four seasons, the results of which are shown in Table 2. The largest observed and simulated Arctic temperature anomalies occur in the January-February-March (JFM) and October-November-December (OND) seasons, while the weakest anomalies occur in the July-August-September (JAS) season. The simulated seasonality is very realistic in this regard when the model is driven by the full changes in boundary forcings. The largest fraction of the Arctic warmth that is explained by sea ice loss occurs in the OND season. There is comparatively little seasonality in the Arctic surface warming in the experiments that do not include sea ice loss. This is physically consistent with the fact that the most depleted state of Arctic sea ice occurs in OND and large surface energy flux anomalies associated with such loss are expected to occur in late fall/early winter.

4. Summary and discussion

A suite of historical atmospheric model simulations using a hierarchy of global boundary forcings has been introduced, and were applied to understanding the cause for extremely warm Arctic surface temperature during 2016. All experiments are based on the ECHAM5 model, span the period 1979–2016, and are routinely updated as part of the Climate of the Twentieth Century Detection and Attribution Project. As part of this project, on-line tools have been generated to permit interactive exploratory analysis of the model data which the user can also download in order to conduct more detailed study via the data repository https://www.esrl.noaa.gov/psd/repository/facts/.

In their Factual (standard AMIP) configuration, the simulations facilitate diagnosis of the role that known variations in global boundary forcings including SSTs, sea ice concentration, and GHG and ozone have played in climate variability since 1979. Availability of a 30-member ensemble permits one to assess the magnitude and pattern of forced signals relative to those arising from purely internal atmospheric variability. In a parallel suite referred to as the Counterfactual configuration, boundary forcings are adjusted to an estimate of their late-19th century condition by removing long-term trends in SSTs, sea ice concentration, GHGs and ozone. The residual boundary forcings so constructed attempt to retain the internal fluctuations of climate drivers such as the ENSO cycle and natural decadal ocean variability. Factual and Counterfactual experiments can then be intercompared in order to estimate effects of long-term change on weather and climate conditions. A third suite of simulations, which were especially useful in addressing causes for the extreme 2016 Arctic warmth, are identical to the Factual runs except that sea ice concentrations are set to a fixed climatological condition. Factual and Clim-Polar experiments are intercompared in order to estimate effects of long-term change in Arctic boundary forcings on global weather and climate conditions, a question of active scientific research and debate (e.g. Cohen et al., 2014; Overland et al., 2016b).

Using these model-based research tools, our study sought to explain the intensity and the timing for extreme Arctic warmth in 2016. The principal result was that much of the magnitude (~3.2 °C) of surface temperature anomalies averaged poleward of 65°N in 2016 was forced by a global pattern of boundary conditions. The ECHAM5 Factual simulations revealed that three quarters of the magnitude of 2016 annual mean Arctic warmth was likely a forced signal, with an even larger fraction when considering reductions in sea ice thickness. The most important driver was Arctic sea ice loss which accounted for 60–70% of the 2016 Arctic warmth, with estimates sensitive to assumptions of sea ice thickness change. About 30–40% of the overall forced warming signal likely arose from drivers outside of the Arctic. Our experiments indicated that the extreme magnitude of the 2016 Arctic warmth could not have occurred without consideration of the Arctic sea ice volume loss. Importantly, Counterfactual experiments indicated that internal variability alone, even of an extreme articulation, could not explain that occurrence of the 2016 extreme warmth. The timing of the event in 2016 is found to be reconcilable with an increasing trend in the overall boundary forced warming – the Factual experiment's ensemble mean Arctic warmth during 2016 exceeded that of any year since 1979. We also repeated our analysis using a second model – CAM5, and confirmed our finding from the ECHAM5 analysis that Arctic boundary condition is a necessary condition to explain the extreme event's magnitude. However, Arctic sea ice loss alone is an insufficient factor in both models revealing that drivers outside the Arctic must also have been necessary factors in causing the 2016 extreme warmth.

While these atmospheric modeling methods provide considerable insights on principal causes for the extreme 2016 Arctic warmth, their design has various shortcomings that make more definitive interpretations difficult. In particular, given that the sea ice loss is identified as a key driver herein, it is important to ascertain its cause. It is almost certain that weather-related atmospheric driving affected sea ice loss in 2016 and contributed to its extreme low volumes (see e.g. Kim et al., 2017), and there is also evidence that about 40% of post-1979 sea ice decline has resulted from internal variability rather than climate change alone (Ding et al., 2017). In this sense, our estimate that at least three quarters of Arctic surface warmth in 2016 was boundary forced, the majority of which was linked to sea ice loss, should not be viewed as an equivalent statement regarding the magnitude of human-induced climate change driving. Our results also reveal that a "true" factual climate simulation should also include changes in observed sea ice thickness and not just changes in sea ice extent.

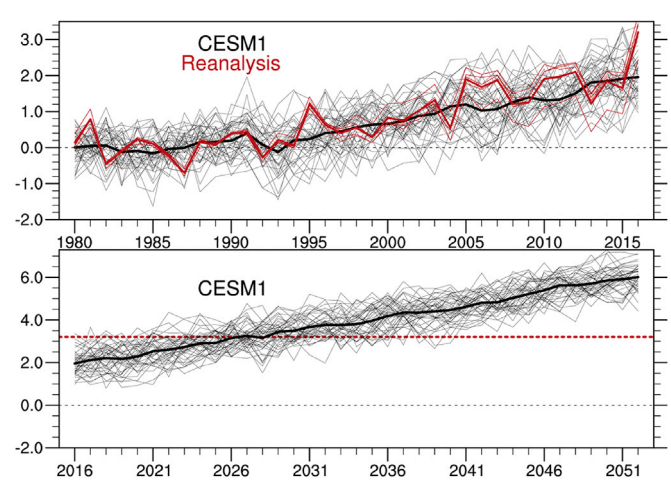

Fig. 6. (Top) As in Fig. 4, but for the CESM1 Large Ensemble subjected to "All Forcings" during historical period and RCP8.5 emission scenario after 2005. (Bottom) Extension of the top panel time series to 2052. The red dashed line denotes the mean of the five reanalysis Arctic surface temperature anomalies in 2016 (3.2 °C).

This issue is clarified by examining Arctic surface temperature time series simulated in a coupled ocean-atmosphere model based on the NCAR Community Earth System Model (CESM1) Large Ensemble that has been forced by the time varying greenhouse gases, aerosols, and volcanic and solar variability (Kay et al., 2015). Figure 6 (top) compares the CESM1 1980–2016 annual Arctic surface air temperature time series (black curves) with the average of reanalysis products (red curve). The spread in Arctic surface air temperatures among the individual runs is appreciably larger (2-fold) compared to that in ECHAM5, which we believe is principally due to coupled internal sea ice variability. The CESM1 2016 Arctic warmth of 2.0 ± 0.2 °C is lower than the ECHAM5 Factual simulation for 2016, even though CESM1 has climate sensitivity greater than the average of CMIP5 models (Hurrell et al., 2013). Based on the ratio of the CESM1 ensemble mean anomaly to the observed temperature anomaly, we are able to estimate that human-induced climate change may have driven about 61% ± 5% of the 2016 Arctic warmth. Such a view is consistent with evidence for an appreciable internal component of the 2016 sea ice loss itself, the result of which that would have been to magnify the warm signal in the ECHAM5 experiments wherein those sea ice conditions were specified. Such an interpretation is consistent with the fact that the observed 2016 warmth is an extreme event relative to the ensemble spread of the CESM1 coupled simulations. The atmospheric and coupled model results for 2016 Arctic warmth are thus reconcilable when considering that the former experiments imposed an Arctic boundary condition having an appreciable internally driven origin.

While internal coupled processes undoubtedly contributed to the extreme magnitude of Arctic warmth in 2016, such a condition is projected to become the typical annual surface temperature within a mere decade, according to the CESM1 projections under an RCP8.5 emissions scenario (Fig. 6, bottom). Further, by the middle of the 21st century, the typical annually averaged Arctic surface temperature anomaly is projected to be nearly doubly that which occurred in 2016. This remarkable rate of warming in the Arctic is closely tied to the projected loss in Arctic sea ice (Jahn et al., 2016). Whereas the role of internal coupled variability was appreciable in explaining the 2016 event intensity, it is clear that by mid-21st Century the forced signal of warmth will far exceed the magnitude of internal variability.

Acknowledgements

The authors thank two anonymous reviewers for their constructive comments that improved the manuscript.

Appendix A. Supplementary data

Supplementary data related to this article can be found at https://doi.org/10.1016/j.wace.2017.11.001.

References

Christidis, N., Stott, P.A., Scaife, A.A., Arribas, A., Jones, G.S., Copset, D., Knight, J.R., Tennant, W., 2013. A new HadGEM3-A-based system for attribution of weather- and climate-related extreme events. J. Clim. 26, 2756–2783. https://doi.org/10.1175/JCLI-D-12-00169.1.

Cionni, I., Eyring, V., Lamarque, J.F., Randel, W.J., Stevenson, D.S., Wu, F., Bodeker, G.E., Shepherd, T.G., Shindell, D.T., Waugh, D.W., 2011. Ozone database in support of CMIP5 simulations: results and corresponding radiative forcing. Atmos. Chem. Phys. Discuss. 11, 10875–10933. https://doi.org/10.5194/acpd-11-10875-2011.

Cohen, J., et al., 2014. Recent Arctic amplification and extreme midlatitude weather. Nat. Geo. 7, 627–637. https://doi.org/10.1038/NGEO2234.

Dee, D.P., et al., 2011. The ERA-Interim reanalysis: configuration and performance of the data assimilation system. Quart. J. R. Meteorol. Soc. 137, 553–597. https://doi.org/10.1002/qj.828.

Deser, C., Phillips, A.S., Alexander, M.A., 2010. Twentieth century tropical sea surface temperature trends revisited. Geophys. Res. Lett. 37, L10701 https://doi.org/10.1029/2010GL043321.

Ding, et al., 2017. Influence of high-latitude atmospheric circulation changes on summertime Arctic sea ice. Nat. Clim. Change 7, 289–295. https://doi.org/10.1038/nclimate3241.

Folland, C., Stone, D., Frederiksen, C., Karoly, D., Kinter, J., 2014. The International CLIVAR Climate of the 20th Century Plus (C20C+) Project: Report of the Sixth Workshop, 19. CLIVAR Exchanges, pp. 57–59.

Franzke, C.L.E., Lee, S., Feldstein, S.B., 2017. Evaluating Arctic warming mechanisms in CMIP5 models. Clim. Dyn. 48, 3247. https://doi.org/10.1007/s00382-016-3262-9.

Gelaro, R., et al., 2017. The modern-era retrospective analysis for research and applications, version 2 (MERRA-2). J. Clim. 30, 5419–5454. https://doi.org/10.1175/JCLI-D-16-0758.1.

Hurrell, J., Hack, J., Shea, D., Caron, J., Rosinski, J., 2008. A new sea surface temperature and sea ice boundary dataset for the Community Atmosphere Model. J. Clim. 21, 5145–5153. https://doi.org/10.1175/2008JCLI2292.1.

Hurrell, J., et al., 2013. The community Earth System Model: a framework for collaborative research. Bull. Am. Meteorol. Soc. 94, 1339–1360. https://doi.org/10.1175/BAMS-D-12-00121.1.

Jahn, Alexandra, Kay, Jennifer E., Holland, Marika M., Hall, David M., 2016. How predictable is the timing of a summer ice-free Arctic? Geophys. Res. Lett. 43 (17), 9113–9120. https://doi.org/10.1002/2016GL070067.

Kalnay, et al., 1996. The NCEP/NCAR 40-year reanalysis project. Bull. Am. Meteorol. Soc. 77, 437–471. https://doi.org/10.1175/1520-0477(1996)077<0437:TNYRP>2.0.CO;2.

Kay, J.E., Deser, C., Phillips, A., Mai, A., Hannay, C., Strand, G., Arblaster, J., Bates, S., Danabasoglu, G., Edwards, J., Holland, M., Kushner, P., Lamarque, J.-F., Lawrence, D., Lindsay, K., Middleton, A., Munoz, E., Neale, R., Oleson, K., Polvani, L., Vertenstein, M., 2015. The community Earth system model (CESM) large ensemble project: a community resource for studying climate change in the presence of internal climate variability. Bull. Am. Meteorol. Soc. 96, 1333–1349. https://doi.org/10.1175/BAMS-D-13-00255.1.

Kim, B.-M., Hong, J.-Y., Jun, S.-Y., Zhang, X., Kwon, H., Kim, S.-J., Kim, J.-H., Kim, S.-W., Kim, H.-K., 2017. Major cause of unprecedented Arctic warming in January 2016: critical role of an Atlantic windstorm. Sci. Rep. 7, 40051 https://doi.org/10.1038/srep40051.

Kobayashi, S., Ota, Y., Harada, Y., Ebita, A., Moriya, M., Onoda, H., Onogi, K., Kamahori, H., Kobayashi, C., Endo, H., Miyaoka, K., Takahashi, K., 2015. The JRA-55 Reanalysis: general specifications and basic characteristics. J. Meteor. Soc. Jpn. 93, 5–48. https://doi.org/10.2151/jmsj.2015-001.

Krinner, G., Rinke, A., Dethloff, K., Gorodetskaya, I.V., 2010. Impact of prescribed Arctic sea ice thickness in simulations of the present and future climate. Clim. Dyn. 35 (4), 619–633. https://doi.org/10.1007/s00382-009-0587-7.

Lang, A., Yang, S., Kaas, E., 2017. Sea ice thickness and recent Arctic warming. Geophys. Res. Lett. 44, 409–418. https://doi.org/10.1002/2016GL071274.

Meinshausen, M., Smith, S.J., Calvin, K.V., Daniel, J.S., Kainuma, M., Lamarque, J.-F., Matsumoto, K., Montzka, S.A., Raper, S.C.B., Riahi, K., Thomson, A.M., Velders, G.J.M., van Vuuren, D., 2011. The RCP greenhouse gas concentrations and their extension from 1765 to 2300. Clim. Change. https://doi.org/10.1007/s10584-011-0156-z (Special Issue).

Neale, R.B., et al., 2010. Description of the NCAR Community Atmosphere Model (CAM5.0). NCAR/TN-486þSTR. NCAR, Boulder, Colo. Available at: http://www.cesm.ucar.edu/models/cesm1.0/cam/docs/description/cam5_desc.pdf.

Overland, J.E., Wang, M., 2016. Recent extreme Arctic temperatures are due to a split polar vortex. J. Clim. 29, 5609–5616. https://doi.org/10.1175/JCLI-D-16-0320.1.

Overland, J.E., Hanna, E., Hanssen-Bauer, I., Kim, S.-J., Walsh, J., Wang, M., Bhatt, U., Thoman, R., 2016a. Surface air temperature. In: Arctic Report Card: Update for 2016. ftp://ftp.oar.noaa.gov/arctic/documents/ArcticReportCard_full_report2016.pdf. (Accessed 12 July 2017).

Overland, J.E., et al., 2016b. Nonlinear response of mid-latitude weather to the changing Arctic. Nat. Clim. Change 6, 992–999. https://doi.org/10.1038/nclimate3121.

Perlwitz, J., Hoerling, M., Dole, R., 2015. Arctic tropospheric warming: causes and linkages to lower latitudes. J. Clim. 28, 2154–2167. https://doi.org/10.1175/JCLI-D-14-00095.1.

Polyakov, I.V., Alekseev, G.V., Bekryaev, R.V., Bhatt, U., Colony, R.L., Johnson, M.A., Karklin, V.P., Makshtas, A.P., Walsh, D., Yulin, A.V., 2002. Observationally based assessment of polar amplification of global warming. Geophys. Res. Lett. 29 (18), 1878. https://doi.org/10.1029/2001GL011111.

Rayner, N.A., Parker, D.E., Horton, E.B., Folland, C.K., Alexander, L.V., Rowell, D.P., Kent, E.C., Kaplan, A., 2003. Global analyses of sea surface temperature, sea ice, and night marine air temperature since the late nineteenth century. J. Geophys. Res. 108 (D14), 4407. https://doi.org/10.1029/2002JD002670.

Rinke, A., Maslowski, W., Dethloff, K., Clement, J., 2006. Influence of sea ice on the atmosphere: a study with an Arctic atmospheric regional climate model. J. Geophys. Res. 111, D16103 https://doi.org/10.1029/2005JD006957.

Roeckner, E., Bäuml, G., Bonaventura, L., Brokopf, R., Esch, M., Giorgetta, M., Hagemann, S., Kirchner, I., Kornblueh, L., Manzini, E., Rhodin, A., Schlese, U., Schulzweida, U., Tompkins, A., 2003. The atmospheric general circulation model ECHAM5. Part I: model description. Max Planck Inst. Meteorol. Rep. 349, 127.

Screen, J.A., Simmonds, I., 2010. The central role of diminishing sea ice in recent Arctic temperature amplification. Nature 464, 1334–1337. https://doi.org/10.1038/nature09051.

Screen, J.A., Deser, C., Simmonds, I., Tomas, R., 2013a. Atmospheric impacts of Arctic sea-ice loss, 1979–2009: Separating forced change from atmospheric internal variability. Clim. Dyn. 43, 333–344. https://doi.org/10.1007/s00382-013-1830-9.

Screen, J.A., Simmonds, I., Deser, C., Tomas, R., 2013b. The atmospheric response to three decades of observed Arctic sea ice loss. J. Clim. 26, 1230–1248. https://doi.org/10.1175/JCLI-D-12-00063.1.

Serreze, M.C., Francis, J.A., 2006. The Arctic amplification debate. Clim. Change 76, 241. https://doi.org/10.1007/s10584-005-9017-y.

Smith, T.M., Reynolds, R.W., Peterson, T.C., Lawrimore, J., 2008. Improvements NOAA's historical merged land–ocean temp analysis (1880–2006). J. Clim. 21, 2283–2296. https://doi.org/10.1175/2007JCLI2100.1.

Solomon, A., Newman, M., 2012. Reconciling disparate twentieth-century Indo-Pacific ocean temperature trends in the instrumental record. Nat. Clim. Change 2, 691–699. https://doi.org/10.1038/nclimate1591.

Tanre, D., Geleyn, J.-F., Slingo, J.M., 1984. First results of the introduction of an advanced aerosol-radiation interaction in the ecmwf low resolution global model. In: Gerber, H., Deepak, A. (Eds.), Aerosols and Their Climatic Effects, pp. 133–177. A. Deepak, Hampton, Va.

van Oldenborgh, G.J., Macias-Fauria, M., King, A., Uhe, P., Philip, S., Kew, S., Karoly, D., Otto, F., Allen, M., Cullen, H., 2017. How rare were the unusually high temperatures around the North Pole in November–December 2016 and how were they influenced by anthropogenic climate change? Online at World Weather Attribution https://wwa.climatecentral.org/analyses/north-pole-nov-dec-2016/. (Accessed 12 July 2017).

Walsh, J., Fetterer, F., Stewart, J.S., Chapman, W.L., 2016. A database for depicting Arctic sea ice variations back to 1850. Geogr. Rev. 107 https://doi.org/10.1111/j.1931-0846.2016.12195.x.

Zhang, J.L., Rothrock, D.A., 2003. Modeling global sea ice with a thickness and enthalpy distribution model is generalized curvilinear coordinates. Mon. Wea. Rev. 131, 845–861. https://doi.org/10.1175/1520-0493(2003)131<0845:MGSIWA>2.0.CO;2.